Biomimetic 3D-printed Composites: Ballistic Impact Resistance with Nacre-Inspired and Tubulane Structures

Adam B. Sacherich[1], Seyed Hamid Reza Sanei[1], Charles E. Bakis[2]
[1]School of Engineering, Pennsylvania State University, The Behrend College, Erie, PA
[2]Department of Engineering Science and Mechanics, Pennsylvania State University, University Park, PA
*Corresponding Author Email: sanei@psu.edu

ABSTRACT

This research delves into nature-inspired designs for creating materials with exceptional impact resistance, leveraging cutting-edge 3D printing techniques. Our composite design features a nacre-like outer layer combined with a tubulane-resembling core, aiming to enhance energy dissipation significantly. By emulating the dense aragonite structure found in natural nacre and the unique porosity of tubulane, we were able to enhance ballistic impact resistance. To validate its effectiveness, we conducted ballistics tests using a 40-grain lead-tipped .22 LR bullet at an initial velocity of 330.7 m/s, with a specialized chronograph setup to measure both initial and post-penetration bullet velocities, quantifying energy absorption precisely. This study opens new frontiers in aviation safety, structural engineering, and personal protective equipment, showcasing the transformative potential of biomimicry and additive manufacturing in advancing public safety and material science.

Keywords: Additive Manufacturing, Ballistic Testing, Nature-Inspired Design, Impact Energy, Biomimetic Composites

DOI: 10.33599/SJ.v60no5.06

1. INTRODUCTION

High-velocity, impact resistant materials are valuable to many industries. In the military and law enforcement space, innovative impact resistant materials are critical to improving personal safety[1-8]. In the aerospace industry, impact resistant structures have the capability to make travel safer and more reliable[7],[9]. Impact resistant structures are commonly produced using composite materials that combine a fiber material within a polymer. These composite structures typically perform well in impact scenarios. However, certain geometries are impossible to produce due to the limits of the traditional composite manufacturing process. Recently, additive manufacturing methods to produce composite materials have shown promising mechanical performance[10-12]. Additive manufacturing (AM) offers a revolutionary solution to this challenge, enabling the creation of complex and intricate designs that were previously unattainable. By leveraging the precision and flexibility of AM, it becomes possible to fabricate structures with optimized geometries tailored for maximum impact resistance.

Biomimicry, the practice of emulating structures found in nature, is one promising pathway to developing impact resistant structures. These structures in nature have had millions of years to change and evolve into high performance structures[13]. While these structures are typically very complex, additive manufacturing can be used to create similar structures[14].

By emulating natural structures, high performance specimens can be created. Structures such as turtle shells, hooves, and horns are all natural structures that have high impact resistance[15-17]. Another such structure is nacre. Nacre is a substance found in the inner layer of some seashells. Nacre is comprised of hard aragonite tablets bonded together with a ductile, organic material[18]. These tablets are roughly 450 nm thick with an interface thickness of 30 nm[19]. These structures are stacked and staggered like a brick-and-mortar wall. Upon impact, the hard tablets within the structure can move slightly, which helps to absorb impact energy[20]. This tablet sliding is the primary deformation mechanism of nacre[19]. This deformation leads to strain hardening, which works to reduce crack propagation in the structure significantly[21]. Mimicking this structure using 3D printing shows promise as a method of creating an impact-resistant structure[22].

Statistical variations have been shown to increase the hardening mechanics of nacre and its overall stability[19]. This statistical variation in the structure can be achieved by modeling the tablet arrangement of nacre as Voronoi polygons[21-22]. Modeling the structure in this manner makes it possible to 3D print. In a drop-weight impact test, a nacre-like geometry constructed with a PLA-TPU material combination performed 120% better under impact than a specimen of equivalent dimensions made from monolithic PLA[22]. The PLA was the tablet material in this setup, while the TPU was the matrix. The same testing was done using nylon as a matrix material instead of TPU, and in this case, the specimen performed 25% better than a monolithic PLA specimen. The failure of the nylon specimen was due to the ductile fracture of the nylon and the debonding of the PLA and nylon[22]. Results may have been improved if steps had been taken to better adhere the nylon to the PLA.

While previous research has investigated the behavior of 3D nacre-like geometry when made of two polymer materials, Continuous Fiber Composite Printing (CFCP) could also be used to produce nacre-like structures. CFCP allows for continuous fibers to be added to a 3D-printed part. The addition of continuous fiber to a 3D printed part has been shown to increase the impact resistance of printed parts by over an order of magnitude[23]. Due to the favorable impact properties of continuous fibers, nacre-like structures manufactured using CFCP may perform better than other nacre-like structures.

Creating scaled up models of certain atomic structures has also been shown as an effective way to create impact resistant 3D printed structures. Structures such as schwarzites, pentadiamond, and stochastic bicontinuous microstructures have all shown potential to behave uniquely when 3D printed compared to traditional structures[24-26]. A common feature between all of these structures was their dependence on the topology of the structure[24],[26],[27]. As a result, the scale at which these structures are produced has little impact on the stress curve of the sample, which drives its energy absorbing characteristics[24],[28]. Additionally, the scale does not determine the Young's modulus of the structure as that is controlled by the material that the structure is constructed from[24].

Another structure atomic structure that has been shown to perform well under impact is the Tubulane. Tubulanes are carbon-based atomic structures that have the bond connections of a tubule[29]. Carbon atoms in this structure all have roughly sp^3 hybridization[29]. The porous structure of Tubulanes performs well in energy absorption scenarios[27]. While the tubulane structure was originally theorized for an atomic scale, the mechanical response of the structure is maintained when implemented on a macro scale[27]. The structure also exhibits layer-based deformation, so the impact resistance scales with the structure's thickness[27]. Previous investigations on tubulane behavior under hyper-velocity impacts found that the tubulane structures produced using PLA showed a penetration depth up to ten times less than those made from monolithic PLA[27]. Additionally, the damage from impact was localized, meaning

cracks did not propagate catastrophically[27]. While research on the behavior of tubulanes under hypervelocity impact exists, there is limited testing of the structures under high-velocity impact.

Sandwich structures can also be produced using 3D printing. Sandwich structures utilize a core structure between two skin layers of a different composition or geometry. The outer plates, which are generally stiffer, increase the structure's bending resistance, while the core material increases energy absorption and compressive strength[30-31]. The sandwich structure was chosen for this research as it allows for the combination of multiple high-performance structures. The nacre-like geometry produced in this research was used as the skin layer to serve as a hard strike plate to resist projectile penetration. The tubulane structure is a ductile core that absorbs impact energy[27]. This combination of a hard strike plate with energy-absorbent backing can also be seen in current design patterns for armor design[1].

In this work, various specimens that utilize nacre-like geometries, tubulanes, and sandwich structures were designed. These designs were then manufactured using additive manufacturing. A test setup was designed to measure the energy absorption of different specimen geometries. High velocity impact testing was then conducted to compare the impact resistance of various structures.

2. SPECIMEN GENERATION

2.1 Specimen Modeling

2.1.1 Nacre

The process used to model the nacre-like geometry was similar to that used by Ko and Tran[21-22]. This process revolved around using a Voronoi cell diagram to determine the shape of tablets in nacre. A Voronoi cell diagram is a method of partitioning a region using polygons where each polygon contains all points closer to that polygon's seed point than all other seed points. To create this diagram, a grid of equally spaced points was generated, as shown in Figure 1(a). The spacing of these points dictates the final size of the Voronoi diagram's polygons. The grid spacing was chosen to be 15 mm. This was the minimum spacing necessary for creating tiles that the Markforged Mark 2 could reinforce with continuous fiber[32].

Each point was offset by a random radius (between 0 and 7.5mm) and random direction (between 0° and 180°) from its original position, as shown in Figure 1(b). This results in a collection of randomly distributed points that are not clumped together. These points were then used as the input to create a Voronoi diagram, shown in Figure 1(c).

A block of material was then modeled in Autodesk Inventor (Autodesk, San Francisco, US). The edges of the Voronoi diagram were then used as guides to cut small slits into the block. These slits instructs Eiger (Markforged, Waltham, US), the slicer software used to prepare the models for printing, to place matrix material along these lines; the remaining spaces are filled with a fiber material to form the nacre tablets. The width of these spaces in the final model is 0.8 mm. The thickness of each tablet is 0.4 mm. This process was repeated to create each layer to create the stacking structure of the nacre. Adjacent layers were shifted by half of the grid spacing to better overlap the tiles. These sheets were then stacked. A 0.4 mm thick layer of matrix material was placed between each sheet of nacre tablets.

This process was implemented using a Python script to generate the 3D models[33]. The SciPy library was used to create the Voronoi diagram[34]. Interaction between Python and the Inventor API was achieved using the PyWin32 library.

The size of tablets in the final model, controlled by the spacing of the original grid of points, was chosen to allow for adequate fiber reinforcement with the Markforged Mark 2 3D printer (Markforged, Waltham, US). Through testing, it was found that smaller tablet sizes below 15 mm would not be correctly reinforced by the Eiger slicing software (Markforged, Waltham, US). The final model is shown in Figure 2(a),(b)

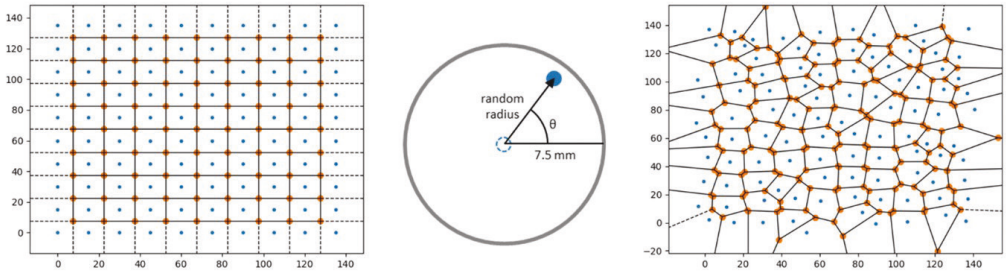

Figure 1. Steps of Voronoi diagram generation: a) a grid of equally spaced points (blue) is created, b) a random angle and radius shift is applied to each point, c) the resulting points are used as the seed points of a Voronoi diagram.

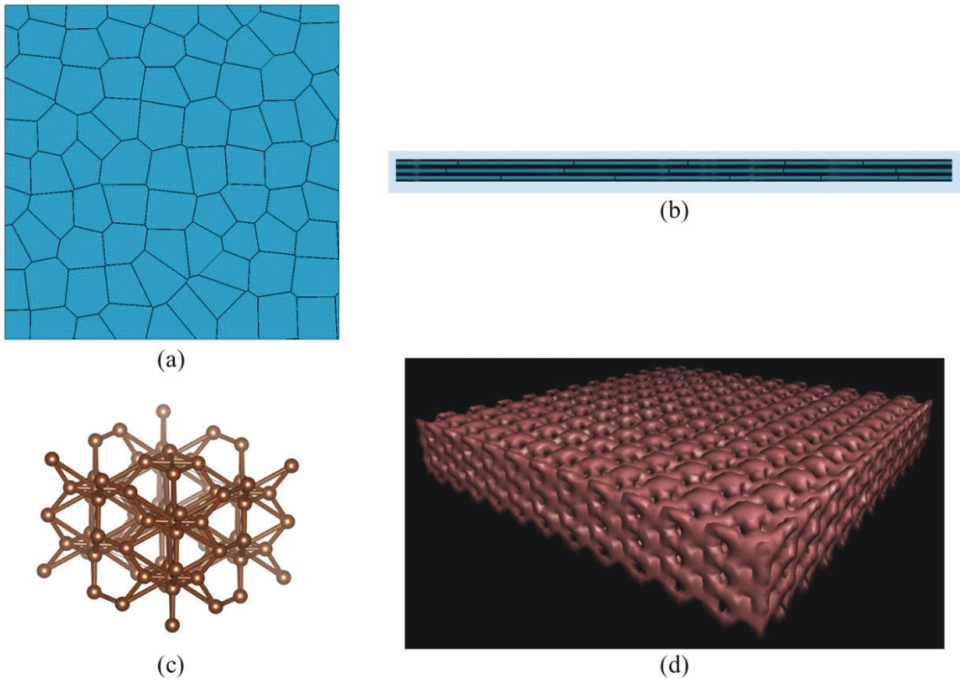

Figure 2. Resulting models from specimen design: (a) Top view of generated nacre-like geometry (tablets are blue, matrix is black), (b) side view of a generated nacre-like geometry that has 3 tablet layers, (c) Tubulane unit cell visualized using VESTA, (d) Output of QuickSurf VMD command.

2.1.2 Tubulanes

The 8-tetra-(2,2) tubulane structure was modeled using a combination of software tools to create an accurate representation. The atomic coordinates provided by Baughman were utilized to generate an atomic structure file in VESTA (CD-FMat, Tsukuba, Japan), a software known for its capability to visualize crystal structures[29]. Figure 2(c) shows the model produced using VESTA. The resulting model was then imported into Visual Molecular Dynamics (VMD) (University of Illinois at Urbana-Champaign, Champaign, US). In VMD, the model was rendered as an STL file using the QuickSurf tool, as shown in Figure 2(d).

3D builder (Microsoft, Redmond, US) was then used to clean and scale the STL model to prepare it for 3D printing. Since the original was in units of nm, the model was upscaled by a factor of 2.2×10^6. This scaling method was chosen as it was the lowest scale factor that could still be manufactured using the Markforged Mark 2 3D printer. The lowest possible scaling factor was selected so that the pore size of the structure is as small as possible relative to the projectile with a diameter of 0.22 in (5.6 mm). The diameter of the pores from the top view is 2.4 mm.

2.1.3 Sandwich Structure

Each specimen had overall dimensions of 125.0 x 125.0 x 20.8 mm. The skin layers were 3.4 mm thick, and the core portion was 14.0 mm thick. According to ASTM E3112[35], a shot-to-edge distance should be at least 51 mm, so this sizing was chosen so that a small round could hit the center of the specimen and not violate this guideline. The part was also made small enough to fit within the build volume of the 3D printers being utilized. To combine the models, the core and skin of the sandwich structure were modeled separately and then combined using 3D builder.

2.1.4 Specimen Configurations

Two batches of specimen configurations were produced. The first batch was designed to test the test setup's functionality and ensure that all geometry could be properly manufactured. The second batch of configurations was put together after the first batch was tested and was designed to address potential issues found after the first round of testing. Configurations 2.1 and 2.2 directly compare the material properties of PLA and Onyx. Configurations 2.2 and 2.3 investigate the benefit of adding skin to a core material. Configurations 2.3 and 2.4 investigate an alternate material combination that may be practical if Onyx underperforms. The gyroid infill pattern used in configuration 2.5 was set to 68% to be equivalent in density to the Tubulane structure. This infill pattern was chosen since it is an available option in all slicing software used and has also been shown to perform well in impact scenarios[36].

A summary of the specimen configurations can be found in Table 1. The nominal mass of each specimen was found using the estimated material usage produced by the Eiger and UltiMaker Cura (UltiMaker, Utrecht, Netherlands) slicing software.

Table 1. Summary of specimen configurations used for testing.

Configuration ID	Core Structure	Core Material	Skin Structure	Skin Material	Nominal Mass (g)	Printer Used
1.1	Tubulane	PLA	Solid	PLA	331.83	FLSUN V400
1.2	Tubulane	Onyx	Nacre	Glass Fiber	329.38	Markforged Mark 2
1.3	50% Gyroid Infill	PLA	None	N/A	158.80	FLSUN V400
2.1	Tubulane	Onyx	None	N/A	194.70	Markforged Mark 2
2.2	Tubulane	PLA	None	N/A	200.37	FLSUN V400
2.3	Tubulane	PLA	Solid	PLA	331.83	FLSUN V400
2.4	Tubulane	TPU	Solid	PLA	326.98	FLSUN V400
2.5	66% Gyroid Infill	PLA	Solid	PLA	194.00	FLSUN V400

2.2 Specimen Manufacturing

Two different printers were used for printing specimens. A Markforged Mark 2 3D printer was used for its ability to print continuous strands of fiber, and a FLSUN V400 (FLSUN, Zhengzhou, China) printer was used to print PLA and TPU.

2.2.1 Markforged Specimens

Markforged Onyx, a nylon material reinforced with chopped carbon fibers, was chosen as the material to use for certain cores and the matrix of nacre-like skin structures for its favorable energy absorption characteristics[37]. For the nacre-like skin structure found in configuration 1.2 (refer to Figure 3), Markforged HSHT Fiberglass was used to form the tablets. This material consists of tows of fiberglass along with an unknown binding agent. The nozzle used for printing Onyx was set to a temperature of 277°C. The nozzle used for printing fiber was set to a temperature of 252°C.

The Eiger slicing software was used to prepare the models for printing on the Markforged Mark 2 3D printer. To get the nacre-like geometry to print correctly, the following adjustments needed to be made:

1. Disabling support material: Support material was not used during printing.
2. Enabling exposed infill: This setting allows for adding fiber near the top and bottom of the print, enhancing structural integrity.
3. Setting the wall layers to 1: The number of wall layers was set to maximize the amount of fiber reinforcement in each tablet.
4. Enabling fiber on all layers containing nacre tablets: Fiber was enabled on every layer that incorporates nacre tablets, ensuring their integration into the composite structure.

2.2.2 FLSUN V400 Specimens

Specimens made from PLA and those containing TPU were produced on an FLSUN V400 printer. Models were prepared using the UltiMaker Cura slicing software. All printing was done with a nozzle temperature of 220°C and a bed temperature of 60°C. To connect PLA skin material with a TPU core material, the print was paused before starting and after finishing the core material so that the material could be changed.

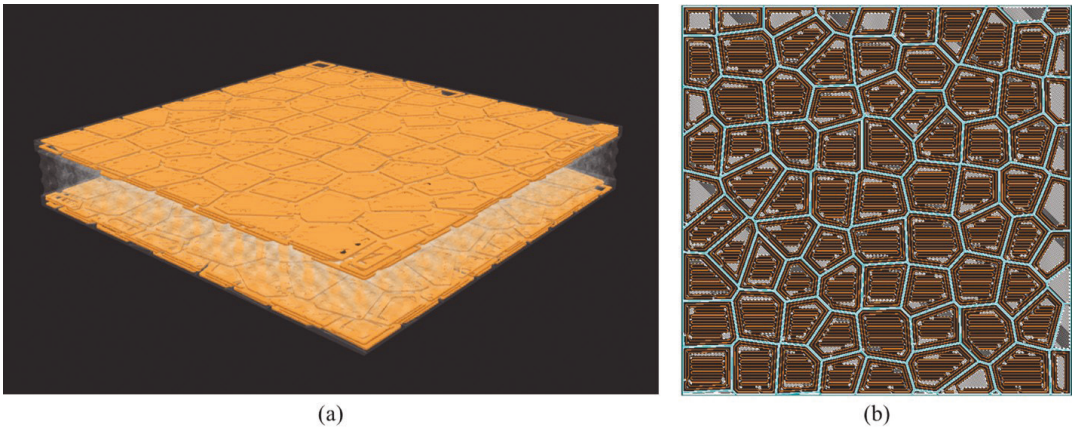

(a) (b)

Figure 3. Fiber placement within the nacre-like geometry: a) Isometric view of HSHT fiberglass (orange) placement. Four layers of tablets were used on each side of the structure. b) Cross-section view of fiber placement within the nacre-like skin structure where orange represents fiber and gray and blue lines represent matrix material. Incomplete tablets near the edge of the part exist due to limitations with the Eiger slicing software but can be ignored as they are far enough away from the point of impact.

3. TEST DESIGN

To test the various specimens, a setup was devised to measure a projectile striking velocity (Vs) and residual velocity (V_R) before and after an impact. The change in kinetic energy of the projectile can be calculated using these velocity measurements along with the projectile's mass. This provides an effective way of measuring the impact energy absorbed by each specimen, allowing for comparisons between configurations.

One existing standard for ballistic impact is the ASTM E3062. This standard outlines specifications for indoor ballistics testing for small arms[38]. The standard defines distances between measurement devices, specimen mounting requirements, and measurement system requirements. Minor modifications were made to this testing standard to fit this experiment better. First, a second pair of velocity measurement devices were added behind the specimen. ASTM E3062 only measures the initial velocity of a projectile, so this second pair of measurement devices is needed to measure the exit velocity. The distance between the specimen and the velocity measurements was also reduced to increase the consistency of the velocity reading of the exiting projectile. Having the measurement devices closer also made it easier to ensure they were aligned correctly.

The ASTM E3112 definition of a fair hit was also used to determine whether a shot was acceptable. To be considered a fair hit, a shot must be 51 mm away from the specimen's edge, and the bullet's yaw must be less than 5°[35]. The shot-to-edge distance was measured with a ruler, and the projectile was measured with a yaw card mounted between 51 mm and 305 mm in front of the specimen.

For the testing, a 0.22 long rifle firearm was employed utilizing 40 grain (2.6 grams) lead round-nose bullet. Projectiles from this setup had a striking velocity of 330.7 m/s. A lead round-nose bullet was chosen as it would have limited deformation upon impact compared to a hollow point or flat nose bullet. Limited deformation ensures that the test specimen absorbs most of the energy instead of the projectile. This size of projectile was chosen because it is a standard size. Since it is smaller than some other standard rounds, the difference in velocity before and after impact should be more exaggerated, which allows for easier comparisons between specimens.

3.1 Test Setup Design

As shown in Figure 4(a),(b), a test setup was designed to measure the entrance and exit velocities of a projectile striking a specimen. This design mounts two chronographs before and two after a rigidly mounted test specimen. Two chronographs were used for each velocity measurement to meet the ASTM E3062 requirement of having two independent velocity measurements. This repeated measurement can be used to ensure that the measured values are accurate. The chronographs and test specimen mount were secured to a 3.8 x 18.4 x 240 cm wooden board. The mounts for the chronographs, as well as the mount for the specimen, are adjustable so that the bullet can travel through the optimal part of the chronograph. All parts of the test setup were constructed from wood and plastic, as metal could pose a safety risk in the event of a shot missing the target.

Chronographs were chosen as the selected form of velocity measurement as they are commonly used for measuring firearm bullet velocities, provide accurate results, and are cost-effective.

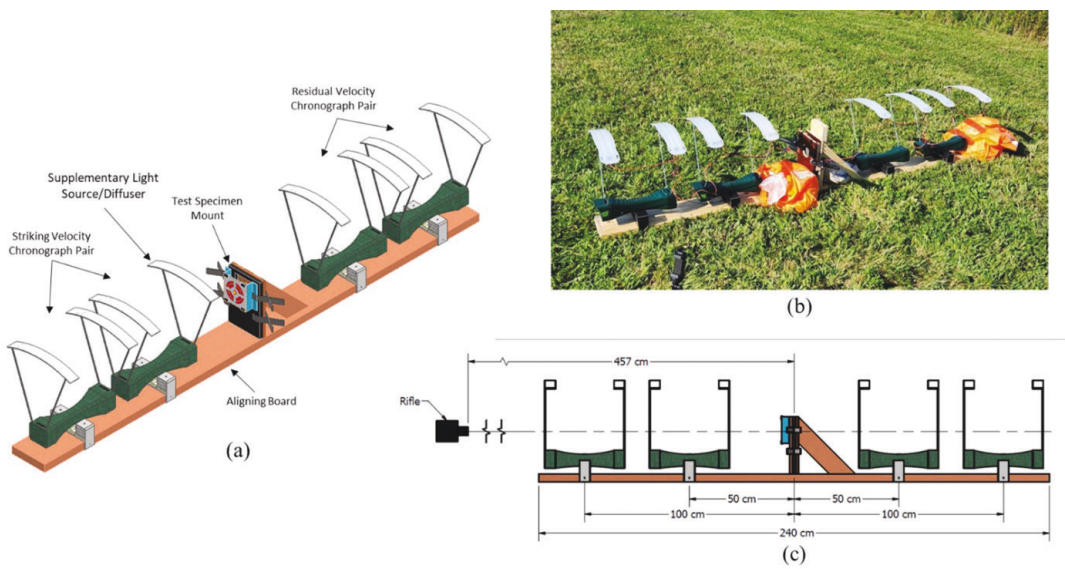

Figure 4. Ballistic test setup: (a) rendering of the test setup, (b) final construction of the test setup, (c) critical distances used for testing.

Chronographs measure the time it takes for a projectile to travel between two optical sensors a known distance apart. The chronograph can then calculate the projectile's velocity using the known distance and recorded time. Velocity measurements of the projectile were performed using four Caldwell Ballistic Precision Chronographs (Caldwell Shooting Supplies, Columbia, US). This chronograph model is factory-calibrated for an accuracy of ±0.25%. Since chronographs are very sensitive to lighting, LED light strips were added to each chronograph to provide additional lighting if environmental lighting is inadequate.

As shown in Figure 4(c), the distance between the front and back pairs of chronographs is the same. The 75 cm between the measurement and the specimen is much smaller than that outlined in ASTM E3062. This reduction in distance was done to allow for better alignment of the chronographs and to increase the likelihood that the exiting projectile travels through the rear chronograph pair. The distance reduction also reduces energy loss due to drag on the bullet before measurement.

3.2 Test Procedure

Before beginning testing:

1. The test setup is placed on level ground.
2. Setup is weighed down using two sandbags.
3. Chronographs are powered on and aligned with one another.
4. A test shot is fired through the setup. If chronographs do not correctly detect the projectile, their height can be adjusted. The lights of the chronograph can also be turned on if the lighting is inadequate.

Testing process:

1. Mount a specimen within the specimen mount and clamp it down to prevent movement.
2. Fire a round into the setup at the appropriate firing distance.
3. Record velocity measurements and remove the specimen from the mounting apparatus.
4. Repeat testing until all test specimens have been impacted.

3.3 Testing Metrics

To comprehensively evaluate the performance of nature-inspired 3D-printed materials under ballistic impact, a series of critical testing metrics were selected for their relevance to assessing impact resistance and energy absorption capabilities. This study examines the performance of the specimen configurations using energy absorption, the ballistic penetration indicator (BPI), and through a visual inspection of the specimen.

Using the striking velocity (V_S), the residual velocity (V_R), and the projectile mass (m_b), the energy absorbed by each specimen (E_a) can be calculated as follows:

$$E_a = \frac{1}{2} m_b \left({V_S}^2 - {V_R}^2 \right) \quad [1]$$

Since energy absorption considers both striking and residual velocity, variations in striking velocity cannot be accounted for by comparing residual velocities alone. However, to compare the structures further, the BPI was calculated using the mass of the specimen (m_s) and the area of the specimen from the top layer (A). The BPI of a specimen serves as a metric for comparison between specimens, as it relates impact energy to the size and mass of a specimen[39]. This allows the specimen that performs best for its weight to be identified. This value can also be compared with other research on ballistic impact. BPI can be calculated as shown below:

$$\mathrm{BPI} = \frac{E_a A}{m_s} \quad [2]$$

After testing is completed, a visual inspection of the test specimens will be performed. This inspection will seek to identify the failure method present in each specimen, such as ductile hole formation, plugging, delamination, discing, conoidal (cone shaped) fracture, comminution, or radial cracking[1]. Determining the specimens' failure mechanism will allow insight into how the specimen could be improved.

It is worth noting that, other common metrics such as crush force efficiency and penetration depth were not applicable here. Crush force efficiency necessitates direct measurement of impact forces to assess how effectively a structure converts impact force into absorbed energy. However, since our testing setup does not measure these forces, this metric could not be calculated. Similarly, penetration depth, commonly utilized in other studies analyzing similar structures, was impractical for our research, which focuses on the complete penetration of projectiles[27].

4. RESULTS

Two rounds of proof-of-concept testing were performed to verify the testing apparatus's functionality and observe the behavior of various specimen configurations. The first round of testing confirmed that the testing apparatus was functional. For this round, four test specimens were each impacted once. The average residual velocity of the projectile was recorded for each specimen. These results are summarized in Table 2 as ID numbers 1.1, 1.2, and 1.3. The striking velocity was not recorded for these tests; only the maximum residual velocity was recorded. The nominal striking velocity of 330.7 m/s was used for E_a and BPI calculations. During this testing, it was found that the setup was sensitive to environmental lighting, and the orientation of the setup relative to the light source influenced the consistency of measurements.

Table 1. Proof of concept findings of ballistic testing. The measurements highlighted in yellow are unacceptable according to ASTM E3062 due to varying by greater than 3 m/s from one another. Only one chronograph measurement was recorded for measurements highlighted in blue.

ID	Specimen	Core Structure	Core Material	Skin Structure	Skin Material	V_S (m/s)	V_R (m/s)	E_a (J)	BPI (m^4/s^2)
1.1	1	Tubulane	PLA	Solid	PLA	330.7*	11	142.0	0.006687
1.2	1	Tubulane	Onyx	Nacre	Fiberglass	330.7*	116	124.7	0.005914
1.3	1	50% Gyroid	PLA	None	N/A	330.7*	287	35.1	0.003470
	2					330.7*	283	38.1	0.003763
2.1	1	Tubulane	Onyx	None	N/A	331/330	248/218	62.5	0.005014
	2					343/342	268/228	59.6	0.004781
2.2	1	Tubulane	PLA	None	N/A	337/337	Err/100	134.6	0.010499
	2					358/355	241/241	91.1	0.007105
2.3	1	Tubulane	PLA	Solid	PLA	348/347	158/67	125.0	0.005885
	2					341/340	84/Err	142.0	0.006686
2.4	1	Tubulane	TPU	Solid	PLA	348/346	254/251	73.6	0.003515
	2					349/348	183/34	114.8	0.005486
2.5	1	68% Gyroid	PLA	None	N/A	342/342	251/248	70.2	0.005453
	2					332/333	244/14	66.8	0.005190

*Calculations were done assuming a nominal striking velocity of 330.7 m/s

The second round of testing involved impacting configuration ID numbers 2.1, 2.2, 2.3, 2.4, and 2.5, as shown in Table 2. For this round of testing, the striking velocity and residual velocity for all four chronographs were recorded. During this testing, not all measured residual velocities fell within 3 m/s of one another (notated by highlighted cells in Table 2). This violates the ASTM E3062 testing standard, which requires the velocity measurement pair to read within 3 m/s of one another. E_a and BPI are still calculated for these tests, but it should be noted that these results may not represent the actual performance of the structures. The higher striking and residual velocity measurements were used for all calculations for each chronograph pair.

Comparing configurations 2.1 and 2.2, it could be concluded that PLA may outperform Onyx as a tubulane material due to its greater BPI. This may suggest that PLA could outperform Onyx as a core material. If so, a specimen configuration utilizing TPU and PLA to make a nacre-like skin could outperform the fiber-reinforced configuration. Comparing the BPI from configurations 2.2 and 2.5 also reveals that the tubulane core material can absorb more energy than a gyroid core. Due to the limited number of data points within the ASTM E3062 standard, more testing would need to be done to confirm these conclusions.

Based on the images shown in Figure 6 and Figure 5, different specimen configurations appear to have different failure mechanisms. The failure of configuration 1.2 shows signs of delamination between the HSHT fiberglass nacre skin and the tubulane core made from Markforged Onyx. Configurations 2.1, 2.2, and 2.3 appear to have failed due to conoidal fracture (shown in Figure 5(b)). In specimen 2.3, the cavity created is 11 mm deep. This is the largest damage area seen on any of the samples. The breaks on these configurations go deeper into the specimens than those on other configurations. This suggests that the bonding between core material layers failed before the material failed. A different failure mechanism was observed in configurations 2.4 and 2.5. The failure of these specimens is more representative of ductile hole formation until the bullet reaches the final layer of the specimen (shown in Figure 5(c),(d)).

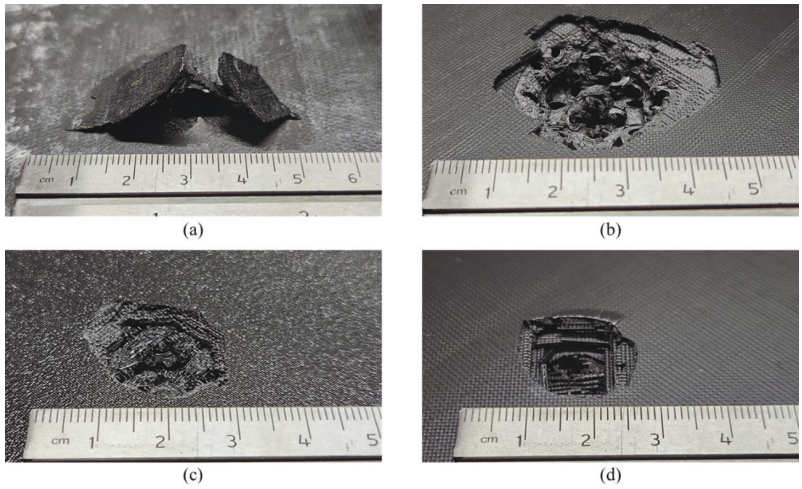

Figure 5. Different failure methods observed on specimens: (a) specimen ID 1.2, (b) specimen ID 2.3, (c) specimen ID 2.4, (d) specimen ID 2.5.

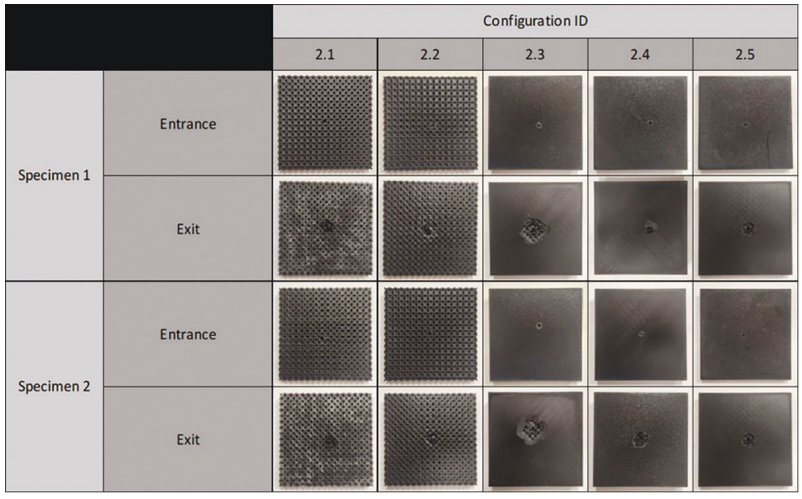

Figure 6. Specimens after impact testing.

5. CONCLUSIONS

In this study, a ballistic test setup was designed to collect data to calculate the impact energy absorption of 3D printed specimen. Various specimen configurations were then modeled, manufactured, and tested. All configurations were able to be produced using commercially available 3D printers. These specimens utilized continuous fiber reinforcement as well as tubulane, nacre-like, and sandwich structures.

Experimentation up to this point has revealed some minor flaws in the test procedure that need to be fixed to get better results. The first issue that needs to be addressed is inconsistent readings from the residual velocity chronographs. This is likely a result of debris from the specimen triggering the chronograph instead of the bullet. Further testing will include a thin sheet placed behind the specimen to combat this. This sheet will catch lower-velocity debris from the specimen and allow the faster-moving bullet to pass through. The energy this sheet absorbs can be calculated by firing a bullet through the setup without a specimen loaded. This amount of energy absorbed would be subtracted from all of the results.

The second potential issue with the setup is that the bullet may not make complete contact with the tubulane structure as it might pass through a more open part of the pore structure. Doing more tests per specimen configuration and firing through different parts of a specimen could reduce the effect of the tubulane pore structure on impact resistance. Additionally, a larger bullet could make the difference between bullet size and pore size greater. This could lead to a better distribution of force across the structure. With the 3D printers used in this work, reducing pore size is not a solution to this problem as the tubulane structure is already being printed at the minimum possible size. However, by utilizing different 3D printers, it may be possible to reduce the pore size of the tubulane structure further.

Further testing will test a more significant number of specimens for each configuration and focus more on how different nacre-like structures interact with core structures. More definitive energy absorption metrics can be gathered by testing more of each configuration to allow for better comparisons between configurations.

ACKNOWLEDGEMENT

The authors would like to express their sincere gratitude to Mr. Joshua Allen Haines for his invaluable assistance in conducting the ballistic testing. His expertise and dedication were instrumental in the success of this study, and the findings presented in this paper would not have been possible without his significant contributions.

6. REFERENCES

[1]. I. G. Crouch, "Introduction to armour materials," in *The Science of Armour Materials*, Elsevier, 2017, pp. 1–54. doi: 10.1016/b978-0-08-100704-4.00001-3.

[2]. L. K. Grunenfelder et al., "Bio-inspired impact-resistant composites," in *Acta Biomaterialia*, Elsevier Ltd, 2014, pp. 3997–4008. doi: 10.1016/j.actbio.2014.03.022.

[3]. J. Huang, H. Durden, and M. Chowdhury, "Bio-inspired armor protective material systems for ballistic shock mitigation," *Mater Des*, vol. 32, no. 7, pp. 3702–3710, Aug. 2011, doi: 10.1016/J.MATDES.2011.03.061.

[4]. A. Dutta, A. Vanderklok, and S. A. Tekalur, "High strain rate mechanical behavior of seashell-mimetic composites: Analytical model formulation and validation," *Mechanics of Materials*, vol. 55, pp. 102–111, Dec. 2012, doi: 10.1016/J.MECHMAT.2012.08.003.

[5]. R. D. Petersen and A. Ouellet, "Law Enforcement Officers Killed in the Line of Duty: Contextual and Situational Factors Relating to Body Armor," *American Journal of Criminal Justice*, vol. 48, no. 1, pp. 218–232, Feb. 2023, doi: 10.1007/S12103-021-09622-Z/METRICS.

[6]. B. Schram, R. Orr, B. Hinton, R. Pope, and G. Norris, "The effects of body armour on the power development and agility of police officers," *Ergonomics,* vol. 62, no. 10, pp. 1349–1356, Oct. 2019, doi: 10.1080/00140139.2019.1648878.

[7]. C. Y. Tham, V. B. C. Tan, and H. P. Lee, "Ballistic impact of a KEVLAR® helmet: Experiment and simulations," Int *J Impact Eng*, vol. 35, no. 5, pp. 304–318, May 2008, doi: 10.1016/J.IJIMPENG.2007.03.008.

[8]. A. Courtney and M. Courtney, "Physical Mechanisms of Soft Tissue Injury from Penetrating Ballistic Impact," Nov. 2012.

[9]. W. Liu and B. Taylor, "Profiles of law enforcement agency body armor policies—A latent class analysis of the LEMAS 2013 data," *J Occup Environ Hyg*, vol. 14, no. 11, pp. 873–881, Nov. 2017, doi: 10.1080/15459624.2017.1339163.

[10]. S. H. R. Sanei and D. Popescu, "3D-Printed Carbon Fiber Reinforced Polymer Composites: A Systematic Review," *Journal of Composites Science*, vol. 4, no. 3, p. 98, 2020, doi: 10.3390/jcs4030098.

[11]. S. H. R. Sanei, A. Arndt, and R. Doles, "Open hole tensile testing of 3D printed continuous carbon fiber reinforced composites," *J Compos Mater,* vol. 54, no. 20, pp. 2687–2695, 2020, doi: 10.1177/0021998320902510.

[12]. D. Hetrick, S. H. R. Sanei, C. E. Bakis, and O. Ashour, "Evaluating the Effect of Variable Fiber Content on Mechanical Properties of Additively Manufactured Continuous Carbon Fiber Composites," *Journal of Reinforced Plastics and Composites*, 2020.

[13]. A. du Plessis et al., "Beautiful and Functional: A Review of Biomimetic Design in Additive Manufacturing," *Addit Manuf*, vol. 27, pp. 408–427, May 2019, doi: 10.1016/J.ADDMA.2019.03.033.

[14]. M. K. Islam, P. J. Hazell, J. P. Escobedo, and H. Wang, "Biomimetic armour design strategies for additive manufacturing: A review," Jul. 01, 2021, *Elsevier Ltd*. doi: 10.1016/j.matdes.2021.109730.

[15]. B. Achrai, B. Bar-On, and H. D. Wagner, "Biological armors under impact—effect of keratin coating, and synthetic bio-inspired analogues," *Bioinspir Biomim,* vol. 10, no. 1, p. 016009, Jan. 2015, doi: 10.1088/1748-3190/10/1/016009.

[16]. J. E. Bertram and J. M. Gosline, "Fracture Toughness Design In Horse Hoof Keratin," *Journal of Experimental Biology*, vol. 125, no. 1, pp. 29–47, Sep. 1986, doi: 10.1242/JEB.125.1.29.

[17]. L. Tombolato, E. E. Novitskaya, P. Y. Chen, F. A. Sheppard, and J. McKittrick, "Microstructure, elastic properties and deformation mechanisms of horn keratin," *Acta Biomater*, vol. 6, no. 2, pp. 319–330, Feb. 2010, doi: 10.1016/J.ACTBIO.2009.06.033.

[18]. F. Barthelat, H. Tang, P. D. Zavattieri, C. M. Li, and H. D. Espinosa, "On the mechanics of mother-of-pearl: A key feature in the material hierarchical structure," *J Mech Phys Solids*, vol. 55, no. 2, pp. 306–337, Feb. 2007, doi: 10.1016/j.jmps.2006.07.007.

[19]. M. Y. Kayacan and A. Üzün, "Ballistic performance of novel design of bulletproof plates inspired by biomimetic approaches," *Polym Adv Technol,* vol. 34, no. 1, pp. 299–316, Jan. 2023, doi: 10.1002/pat.5888.

[20]. A. Ghazlan, T. Ngo, T. Van Le, T. Nguyen, and A. Remennikov, "Blast performance of a bio-mimetic panel based on the structure of nacre – A numerical study," *Compos Struct*, vol. 234, Feb. 2020, doi: 10.1016/j.compstruct.2019.111691.

[21]. P. Tran, T. D. Ngo, A. Ghazlan, and D. Hui, "Bimaterial 3D printing and numerical analysis of bio-inspired composite structures under in-plane and transverse loadings," *Compos B Eng*, vol. 108, pp. 210–223, Jan. 2017, doi: 10.1016/j.compositesb.2016.09.083.

[22]. K. Ko, S. Jin, S. E. Lee, and J. W. Hong, "Impact resistance of nacre-like composites diversely patterned by 3D printing," *Compos Struct,* vol. 238, Apr. 2020, doi: 10.1016/j.compstruct.2020.111951.

[23]. D. R. Hetrick, S. H. R. Sanei, O. Ashour, and C. E. Bakis, "Charpy impact energy absorption of 3D printed continuous Kevlar reinforced composites," *J Compos Mater*, vol. 55, no. 12, pp. 1705–1713, May 2021, doi: 10.1177/0021998320985596.

[24]. S. M. Sajadi et al., "Multiscale Geometric Design Principles Applied to 3D Printed Schwarzites," *Advanced Materials*, vol. 30, no. 1, Jan. 2018, doi: 10.1002/adma.201704820.

[25]. L. C. Felix et al., "Mechanical properties of 3D-printed pentadiamond," *J Phys D Appl Phys*, vol. 55, no. 46, Nov. 2022, doi: 10.1088/1361-6463/ac91dc.

[26]. R. S. Ambekar et al., "Atomic Scale Structure Inspired 3D-Printed Porous Structures with Tunable Mechanical Response," *Adv Eng Mater*, 2021, doi: 10.1002/adem.202001428.

[27]. S. M. Sajadi et al., "3D Printed Tubulanes as Lightweight Hypervelocity Impact Resistant Structures," *Small,* vol. 15, no. 52, Dec. 2019, doi: 10.1002/smll.201904747.

[28]. V. Gaal et al., "Mechanical properties of 3D printed macroscopic models of schwarzites," *Nano Select,* vol. 3, no. 2, pp. 450–458, Feb. 2022, doi: 10.1002/nano.202100147.

[29]. R. H. Baugbman and D. S. Galvgo, "Tubulanes: carbon phases based on cross-linked fullerene tubules," 1993.

[30]. H. Yazdani Sarvestani, A. H. Akbarzadeh, A. Mirbolghasemi, and K. Hermenean, "3D printed meta-sandwich structures: Failure mechanism, energy absorption and multi-hit capability," *Mater Des*, vol. 160, pp. 179–193, Dec. 2018, doi: 10.1016/j.matdes.2018.08.061.

[31]. A. Ghazlan, T. Ngo, P. Tan, Y. M. Xie, P. Tran, and M. Donough, "Inspiration from Nature's body armours – A review of biological and bioinspired composites," Jan. 15, 2021, *Elsevier Ltd*. doi: 10.1016/j.compositesb.2020.108513.

[32]. "Carbon Fiber Composite 3D Printer: Markforged Mark Two." Accessed: Nov. 29, 2022. [Online]. Available: https://markforged.com/3d-printers/mark-two

[33]. G. Van Rossum and F. L. Drake Jr, *Python reference manual.* Centrum voor Wiskunde en Informatica Amsterdam, 1995.

[34]. P. Virtanen et al., "SciPy 1.0: Fundamental Algorithms for Scientific Computing in Python," *Nat Methods*, vol. 17, pp. 261–272, 2020, doi: 10.1038/s41592-019-0686-2.

[35]. "Standard Test Method for Ballistic-resistant *Products and Shoot Packs 1*", doi: 10.1520/E3112_E3112M-20.

[36]. C. Silva, A. I. Pais, G. Caldas, B. P. P. A. Gouveia, J. L. Alves, and J. Belinha, "Study on 3D printing of gyroid-based structures for superior structural behaviour," *Progress in Additive Manufacturing*, vol. 6, no. 4, pp. 689–703, Dec. 2021, doi: 10.1007/s40964-021-00191-5.

[37]. "Material Datasheet Composites," Watertown, MA, Jan. 2022. Accessed: May 17, 2023. [Online]. Available: https://www-objects.markforged.com/craft/materials/CompositesV5.2.pdf

[38]. "Standard Specification for Indoor Ballistic Test Ranges for Small Arms and Fragmentation Testing of Ballistic-resistant Items 1", doi: 10.1520/E3062_E3062M-20.

[39]. Q. Wei, B. Gu, and B. Sun, "Ballistic penetration damages and energy absorptions of stacked cross-plied composite fabrics and laminated panels," Sep. 01, 2020, *SAGE Publications Ltd*. doi: 10.1177/1056789520927074.